Energy Harvesting and Computation Offloading for UAV-assisted MEC with NOMA in IoT Network

Gia-Huy Nguyen, Anh-Nhat Nguyen, Hien-Hieu Le, and Tien-Dung Do

Department of Computing Fundamentals, FPT University, Hanoi 10000, Vietnam
{huynghe180064, hieulhhe181040, dungdthe170502}@fpt.edu.vn
nhatna3@fe.edu.vn

Abstract. This study investigates a unmanned aerial vehicle (UAV)-assisted non-orthogonal multiple access (NOMA) based on mobile edge computing (MEC) in Internet of Things (IoT) networks. Specifically, we consider two IoT device (ID) clusters with resource limits and a UAV with a MEC server operating as a wireless power transfer (WPT) station. We present a protocol termed time switching (TS) - UAV NOMA MEC energy harvesting (EH) (TS-UNME), which includes four phases: energy harvesting, task-offloading, task-computing, and task-downloading. For system performance evaluation, we propose a closed-form expression of successful computation probability (SCP) that accounts for imperfect channel state information (ICSI) across the Rayleigh fading channel. In addition, we present a system performance optimization problem, which optimizes SCP by establishing time switching ratio (TSR) and height of UAV. An particle swarm optimization (PSO)-based approach is utilized for solving the problem. Finally, Monte-Carlo simulations confirm our analysis's precision.

Keywords: internet of things · unmanned aerial vehicles · energy harvesting · nonorthogonal multiple access · mobile edge computing · particle swarm optimization.

1 Introduction

Technology has advanced with some spectacular successes in all industries over the years, particularly in Internet of Things (IoT) with the advent of smart sensor devices such as smart automobiles, smartphones, and computers [1]. However, IoT networks have faced problems such as distance and transmitting data from IoT device (ID). Furthermore, ID's limited battery life and lack of computing power pose difficult challenges.

To address these issues, wireless power transfer (WPT) and mobile edge computing (MEC) have emerged as viable techniques for addressing compute task and device energy. Using MEC's intense computing, IDs offloads part or all of their jobs to servers placed at the edge networks. This helps IoT systems to tremendously reduce their overall latency, and enhance the quality of

communication links [2]. Another issue with IDs are the accompanying short-life batteries. Hence, WPT is a possible choice for resolving this issue [3]. Using the radio frequency (RF) EH, which enables IDs to harvest energy from external sources. For example, Zhou *et al.* [4] summarized the approaches of simultaneous wireless information and power transfer (SWIPT) compared with conventional EH can provide a long-term and sustainable power source for IDs. Hu *et al.* [5] studied a scheme in which mobile terminals were powered by an access point (AP)-assisted MEC with WPT, and they used the harvested power for offloading tasks to AP. Utilizing MEC and WPT technologies, as a result, can minimize the energy consumption and extend the battery-powered capacity of IDs [6].

Nonetheless, the fixed infrastructure in the IoT system has limited transmission coverage and can experience path-loss communications between components due to the urban environment's high building density. Due to its high maneuverability and cost-effectiveness, UAVs are utilized to support IoT infrastructure and IDs in the transmission of information [7]. However, due to the presence of obstacles, large-scale fading conditions may cause inefficient propagation between UAV and IDs. To overcome this, Bithas *et al.* [8] designed a new UAV selection policy, which exploits the best UAV's received signal. Additionally, the IDs offloads their tasks to the UAV that is integrated with the MEC server in order to increase effective processing time and decrease communication latency. In addition, WPT enables UAV to serve as a mobile power-supply station for ground users, resulting in increased energy efficiency of IDs [9].

Furthermore, non-orthogonal multiple access (NOMA) permits an enormous number of mobile devices to simultaneously access IoT network and radio resources by exploiting multiple power domains [10]. In other terms, NOMA has the advantages of transmitting an extraordinarily large amount of data and enhancing spectral efficiency in comparison to other wireless networks such as orthogonal multiple access (OMA) [11]. Combining NOMA with the UAV-assisted MEC model enhances the transmission and calculation capabilities in IoT networks. Kota and Naidu [12] proposed a hybrid NOMA based UAV aided MEC network, which aims to minimize the offloading energy consumption. The results showed that the modified NOMA model's performance outperforms OMA and NOMA scenarios on reducing power usage.

Motivated by the previous discussions, this paper investigates the UAV-aided NOMA based on MEC, in which UAV acts as a power-supply station. We consider that IDs would harvest energy RF from the UAV in order to offload tasks. In addition, we evaluate Line-of-Sight (LoS) and Non Line-of-Sight (NLoS) probabilities between UAV and IDs wireless communication over the Rayleigh fading channel, as well as the effect of imperfect channel state information (ICSI). The following are the primary contributions of our paper:

- We investigated UAV-assisted NOMA based on MEC in IoT networks. In addition, we considered the ICSI for model evaluations in realistic implementations. Consequently, we presented a communication protocol that would guarantee an effective EH and dispatching procedure.

– We derived a SCP closed-form expression for the whole system. In addition, we formulated a problem for maximizing SCP by optimizing EH time of IDs and UAV's height. The problem was solved using a PSO-based algorithm.
– To confirm the efficacy of our system, numerical results were used to evaluate the system's offloading performance, including transmit power of UAV, the number of ID in two clusters, EH time of ID and height of UAV.

The rest of this paper is structured as follows. Section 2 introduces the system model and time-switching protocol. Section 3 analyzes the SCP and optimization for maximum SCP. In Section 4, numerical results are presented and discussed. Finally, conclusions are presented in Section 5.

2 System model and communication protocol

2.1 System and channel model

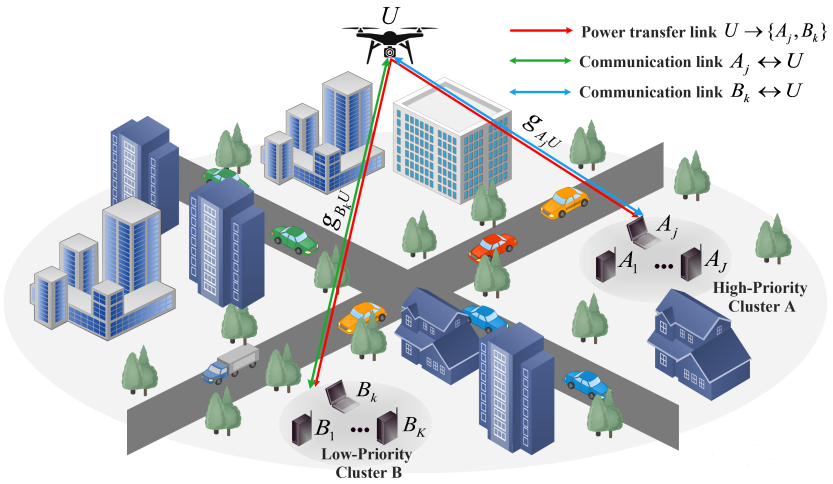

Fig. 1: System model for the UAV-assisted NOMA MEC in IoT networks.

As shown in Fig. 1, we consider an UAV-aided NOMA based on MEC in IoT networks, which consists of cluster A having J high-priority devices, denoted by $A_j, j \in (1, ..., J)$ and cluster B having K low-priority devices, denoted by $B_k, k \in (1, ..., K)$ in transmitting tasks to a UAV denoted by U, where U is equipped with a MEC server for computation and assisted WPT. We consider this IoT system is in a half-duplex mode. The IDs are assumed to be executing the same workloads comprising tasks of length l (bits), in which these distinct tasks are separated into discrete groups [6]. Hence, the offloading capacity of $I_i, I \in (A, B), i \in (j, k)$ is expressed as $\mathcal{L}_i^{off} = \beta_i l$, where $0 \leq \beta \leq 1$.

We adopt a 3D Cartesian coordinate system, where $U(x_U, y_U, h_U)$ with the height $h_U > 0$, $A_j(x_j, y_j, 0)$, and $B_k(x_k, y_k, 0)$. Taking into consideration the LoS and NLoS probabilities between U and IDs links, the mean path loss is calculated as follows [6]:

$$\bar{L}_{ab} = \left[K^{nlos} + \frac{K^{los} - K^{nlos}}{1 + \omega_1 e^{-\omega_2(\theta_{ab} - \omega_1)}} \right] d_{ab}^{\varphi}, \tag{1}$$

where $ab \in \{A_jU, B_kU\}$; $K^{los} = \xi^{los}\left(\frac{c}{4\pi f_c}\right)^{-1}$; $K^{nlos} = \xi^{nlos}\left(\frac{c}{4\pi f_c}\right)^{-1}$; φ is the path-loss exponent; ξ^{los} and ξ^{nlos} are excessive path-losses of LoS and NLoS communication between U and IDs clusters; c is the speed of light; f_c is the carrier frequency; ω_1 and ω_2 are the environmental parameters; $\theta_{ab} = \frac{180}{\pi} \arcsin(\frac{h_U}{d_{ab}})$ is the elevation angle; $d_{ab} = \sqrt{(x_b - x_a)^2 + (y_b - y_a)^2 + h_U^2}$ is the distance of ab. Assuming that channel coefficients follow Rayleigh fading which is modeled by using the minimum mean square error channel estimation error as in [7], expressed as $g_{ab} = \hat{g}_{ab} + \varepsilon_{ab}$, where $\hat{g}_{ab}$ is the estimated channel coefficient; ε_{ab} is the estimated channel error, and $\varepsilon_{ab} \sim \mathcal{CN}(0, \Omega_{ab})$. Supposing that the Ω_{ab} parameter is constant [13]. The best ID in two clusters is selected such that the best possible channel gain of the $U - A_j$ and $U - B_k$ link is achieved as $|\hat{g}_{i^*}|^2 = \max\limits_{i^* \in (j^*, k^*)} \left\{ |\hat{g}_{I_i U}|^2 \right\}$. Due to the effect of Rayleigh distribution, the cumulative distribution function (CDF) and probability density function (PDF) of channel power gains $|\hat{g}_{i^*}|^2$ can be respectively expressed as:

$$F_{|\hat{g}_{i^*}|^2}(x) = \sum_{t=0}^{N} \binom{N}{t} (-1)^t e^{-\frac{tx}{\lambda_x}}, \tag{2}$$

$$f_{|\hat{g}_{i^*}|^2}(x) = \sum_{t=1}^{N} \binom{N}{t} \frac{(-1)^{t+1} t}{\lambda_x} e^{-\frac{tx}{\lambda_x}}, \tag{3}$$

where $N \in (J, K)$, $t \in (k, p)$.

2.2 Communication protocol

In this sub-section, we discussed the TS protocol system given in Fig. 2. The following is the detail description for each phase of the protocol:

- In the first phase t^{eh}, IDs harvest energy from the UAV, which can be expressed as $E_i = \frac{\eta P_U \alpha T \left(|\hat{g}_{i^*}|^2 + \Omega_{i^*}\right)}{\bar{L}_i}$, where η is the EH efficiency coefficient, $0 < \eta < 1$; P_U is UAV transmission power; α is the TS ratio, $0 < \alpha < 1$; T is the transmission block time.
- In the second phase $t_{i^*}^{off}$, A_{j^*} and B_{k^*} simultaneously offload $\mathcal{L}_{j^*}^{off}$ and $\mathcal{L}_{k^*}^{off}$ to U using uplink NOMA. Therefore, the signal retrieved at U is as follows:

$$\gamma_U^{MEC} = \sqrt{\frac{P_{j^*}}{\bar{L}_{j^*}}} \left(\hat{g}_{j^*} + \varepsilon_{j^*}\right) x_{j^*} + \sqrt{\frac{P_{k^*}}{\bar{L}_{k^*}}} \left(\hat{g}_{k^*} + \varepsilon_{k^*}\right) x_{k^*} + n_U, \tag{4}$$

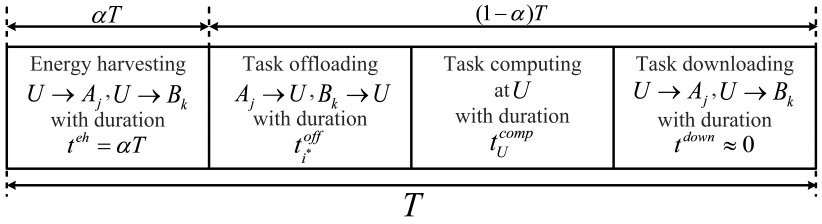

Fig. 2: The TS-UNME protocol.

where $P_{i^*} = \frac{E_{i^*}}{(1-\alpha)T - t_U^{comp}}$ is the power transmit; x_{j^*} and x_{k^*} are the two best transmitted signal of A_{j^*} and B_{k^*}; $n_U \sim \mathcal{CN}(0, N_0)$. Here, U decodes x_{j^*} by considering x_{k^*} as interference. Subsequently, U decodes x_{k^*} by canceling out the known x_{j^*} by successive interference cancellation (SIC) [6]. Hence, the retrieved signal-to-interference-plus-noise ratios (SINRs) for detecting x_{j^*} and x_{k^*} are expressed as [14] $\gamma_{j^*}^U = \frac{a_1 x^2}{a_2 y^2 + a_3}$, $\gamma_{k^*}^U = \frac{a_4 y^2}{a_5}$, respectively, where $x = |\hat{g}_{j^*}|^2$, $y = |\hat{g}_{k^*}|^2$, $a_1 = \gamma_{j^*}\overline{L}_{k^*}$, $a_2 = \gamma_{k^*}\overline{L}_{j^*}$, $a_3 = a_2\Omega_{k^*}^2 + a_1\Omega_{j^*}^2 + \overline{L}_{j^*}\overline{L}_{k^*}$, $a_4 = \frac{\gamma_{k^*}}{\overline{L}_{k^*}}$, $a_5 = a_4\Omega_{k^*}^2 + 1$, $\gamma_{j^*} = \frac{\eta\gamma_U \alpha T}{\overline{L}_{j^*}[(1-\alpha)T - t_U^{comp}]}$, $\gamma_{k^*} = \frac{\eta\gamma_U \alpha T}{\overline{L}_{k^*}[(1-\alpha)T - t_U^{comp}]}$, $\gamma_U = \frac{P_U}{N_0}$.

- In the third phase, the offloaded tasks are computed by MEC sever at U, and the time t_U^{comp} needed to execute all the task bits at U is given as $t_U^{comp} = \frac{(\mathcal{L}_{j^*}^{off} + \mathcal{L}_{k^*}^{off})\mathbb{C}}{f_U^{mec}}$, where $\mathbb{C}$ is the number of CPU cycles requires for calculating a task bit; f_U^{mec} is the hosting frequency of MEC sever.
- In the fourth phase, the processed results are sent back to A and B clusters. Due to the extremely short delay-time and low energy requirement for returning the data, we assumed t^{down} is approximately equals to 0 [15].

3 System Performance

3.1 Successful Computation Probability

In this subsection, we proposed the concept of SCP designed as the likelihood for successful computation of all offloaded task bits within T^{th} time latency. The system SCP is formulated as follows:

$$SCP_s = \Pr\left\{\max\left(t_{j^*}^{off}, t_{k^*}^{off}\right) < T^{th}\right\}, \tag{5}$$

where $T^{th} = (1-\alpha)T - t_U^{comp}$, $t_{i^*}^{off} = \frac{\mathcal{L}_{i^*}^{off}}{C_{i*}}$; $C_{i*} = WT^{th}\log_2\left(1+\gamma_{i^*}^U\right)$ is the channel capacity; W is the bandwidth.

Lemma 1. *The closed-form expression of the SCP for the UAV-aided NOMA based MEC system under Rayleigh fading channel is given by:*

$$SCP_s = \sum_{p=1}^{K} \binom{K}{p} \frac{(-1)^{p+1} p}{\lambda_y} \left[\frac{\lambda_y e^{-\frac{p}{\lambda_y} B}}{p} - \frac{\pi b}{2Z} \sum_{k=0}^{J} \binom{J}{k} (-1)^k \sum_{z=1}^{Z} \sqrt{1-(\zeta_z)^2} e^{-\frac{k}{\lambda_x} A} {\omega_z}^{\frac{p}{\lambda_y}-1} \right], \quad (6)$$

where $B = \sqrt{\frac{\sigma_B a_5}{a_4}}$, $A = \sqrt{\frac{\sigma_A [a_2(-\ln(\omega_z))^2 + a_3]}{a_1}}$, $b = e^{-B}$, $\zeta_z = \cos\left(\frac{\pi(2z-1)}{2Z}\right)$, $\omega_z = \frac{(\zeta_z+1)b}{2}$, $\sigma_B = 2^{\frac{\mathcal{L}_{k^*}^{off}}{W(T^{th})^2}} - 1$, $\sigma_A = 2^{\frac{\mathcal{L}_{j^*}^{off}}{W(T^{th})^2}} - 1$, *and* Z *is the complexity-vs-accuracy trade-off coefficient [16].*

Proof. See Appendix A.

3.2 Particle swarm optimization for the system SCP

In this subsection, we introduced a solution to maximize the SCP in **Lemma 1.** by obtaining the optimal TSR, denoted as α^*, and the height of UAV, represented as h_U^*. Hence, the SCP optimization problem is given as:

$$\begin{aligned} \underset{h_U, \alpha}{\text{maximize}} \quad & SCP_s \\ \text{subject to} \quad & 0 \le \alpha \le 1, && \text{(7a)} \\ & 0 \le h_U \le h_U^{\max}, && \text{(7b)} \end{aligned}$$

where the conditions of TSR and the UAV height is described in constraints (7a) and (7b). The step-by-step pseudocode of PSO is given in **Algorithm 1.**

4 Numerical result

In this section, we discussed the simulation results that verified our analysis of the SCP for UAV-aided NOMA-MEC in IoT networks under the effect of ICSI over Rayleigh fading channels. The values for all system parameters of the simulations is specified in the following: $x_U = 0$, $y_U = 0$, $h_U \in (0, 80)$; $A(35, 35, 0)$; $B(20, 20, 0)$; $\omega_1 = 0.1581$, $\omega_2 = 9.6177$; $\xi^{los} = 1$, $\xi^{nlos} = 20$; $c = 3.10^8$; $f_c = 10^5$ (Hz); $W = 10^6$ (Hz); $\gamma_U \in (0, 20)$ (dB); $\alpha \in (0, 1)$; $\eta = 0.85$; $T = 1$ (s); $\varphi = 2$; $l = 10^4$; $\beta_{j^*} = 0.6$, $\beta_{k^*} = 0.4$; $f_U = 10^8$ (Hz); $\mathbb{C} = 10^2$; $Z = 10^2$.

4.1 The impact of γ_U on SCP

Fig. 3 illustrates the influence of signal-to-noise ratio (SNR) transmission and the number of IDs on the SCP of the whole system. The result indicates that

Algorithm 1 SCP Maximization based on PSO

Initialize values for parameters: ∂, μ_1, μ_2, Q, $Iter_{max}$;
Set random values for the particle positions and velocity $\mathcal{X}_i$, $\mathcal{V}_i$;
Initialize the local and global best positions: $\mathcal{P}_i$, $\mathcal{S}_i$;
For loop q to $Iter_{max}$ until the condition is met
for each particle $i = 1$ to Q **do**
    Select random numbers for r_1, r_2 values between [0,1]
    Update new position using $\mathcal{X}_i^{q+1} = \mathcal{X}_i^q + \mathcal{V}_i^{q+1}$
    Update new velocity using $\mathcal{V}_i^{q+1} = \partial \mathcal{V}_i^q + \mu_1 r_1 \left(\mathcal{P}_i^q - \mathcal{X}_i^q\right) + \mu_2 r_2 \left(\mathcal{S}_i^q - \mathcal{X}_i^q\right)$
    Update the best personal position:
    if $f(\mathcal{X}_{i+1}^q) \geq \mathcal{P}_i^q$ **then**
        $\mathcal{P}_{i+1}^q = \mathcal{X}_{i+1}^q$
    end if
    if $f(\mathcal{X}_{i+1}^q) < \mathcal{P}_i^q$ **then**
        $\mathcal{P}_{i+1}^q = \mathcal{P}_i^q$
    end if
    Update the best global position:
    $\mathcal{S}_i^q = \max(\mathcal{P}_i^q)$
    if $f(\mathcal{X}_i^q) \geq \mathcal{S}_i^q$ **then**
        $\mathcal{S}_i^q = \mathcal{X}_i^q$
    end if
    $q \leftarrow q + 1$
end for
Return: $f(\mathcal{S}_i^q)$ is the maximum value of SCP

the simultaneous augmentation in IDs' number leads to the improvement of SCP's performance, as the UAV will have greater options to select the best ID from the two clusters. Additionally, the augmentation of γ_U improves SCP outcome because UAV provides more energy for IDs to efficiently offload duties. Moreover, the performance of SCP under the influence of perfect channel state information (PCSI) is superior to that of ICSI. In practice, however, obtaining PCSI is extremely challenging.

4.2 The impact of TS ratio and height of UAV on SCP

Fig. 4 illustrates the impact of EH time and UAV's altitude on system performances. Specifically, Fig. 4a depicts the effect of TS ratio on SCP. The result shows that there is an ideal point of TS ratio α^* that maximizes SCP outcome, because increasing TS ratio allows IDs to spend more time on harvesting energy and less time on communication with the UAV. However, reducing the time spent on EH phase leads to slower task-offloading process, resulting in the poor SCP performance. Therefore, there always exists a α^* at which the SCP obtains its desirable value. Fig. 4b shows the impact of the UAV height on SCP. We can observe that the simulation has an optimal height h_U^* at which SCP reaches its best value. This is because the LoS probability becomes greater when the height

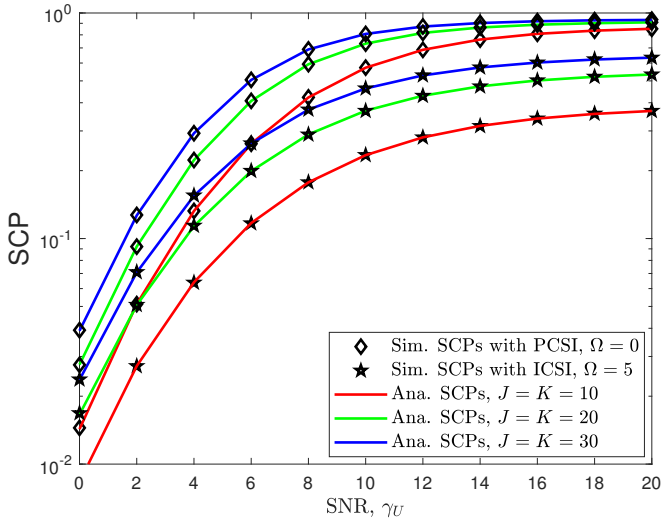

Fig. 3: The impact of γ_U on SCP of the whole system with a different J, K considering PCSI and ICSI.

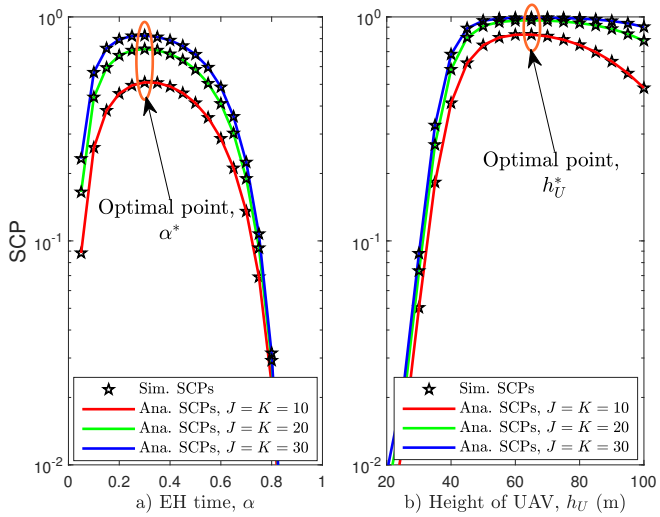

Fig. 4: The impact of TS ratio α in (a) and height of UAV h_U in (b) on SCP of the whole system

of U is increased. However, if UAV exceeds the optimal height value, the SCP performance is decreased due to the enlarged distance between U and IDs.

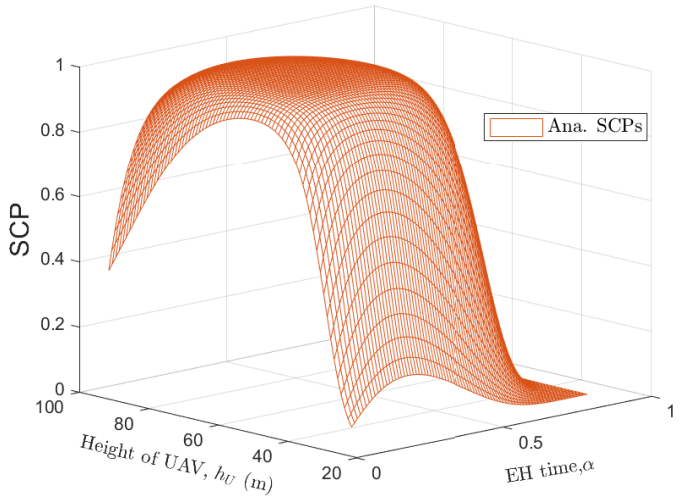

Fig. 5: The impact of both TS ratio and height of UAV on SCP.

Fig. 5 depicts the effects of TS ratio α and h_U on SCPs. We have simultaneously ran the results in Fig. 4a and Fig. 4b, and have generated a 3D simulation considering both α and h_U. The result reveals the existence of the desirable α^* and h_U^* value to achieve the greatest SCP's value. By applying the **Algorithm 1**, introduced in Subsection 3.2, we obtain α^* and h_U^* value in Fig. 6.

4.3 The impact of optimal TS ratio and height of UAV on SCP

In Fig. 6, we compare the SCP performance at the desirable point of α^* and h_U^*, given on the simulation, with different fixed values of TS ratio and UAV's height. We can see that EH time and the optimal UAV's altitude of IDs return the best value for the SCPs.

5 Conclusion

In this paper, the offloading performance of a UAV-assisted NOMA MEC in IoT over Rayleigh fading was investigated. We proposed a four-phased protocol based on UAV-enabled WPT with an emphasis on NOMA-MEC techniques to improve offloading performance. For system performance evaluation, we obtained closed-form expressions of SCP for the entire system. To maximize the SCP, we also proposed a PSO-based algorithm for determining the altitude of a UAV and the EH time of ID. We provided simulation results to confirm the system outsourcing performance.

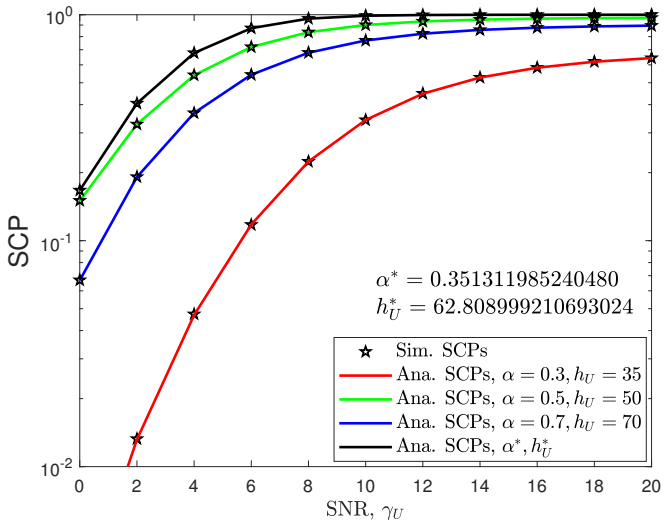

Fig. 6: The impact of optimal UAV's height and EH time on SCP.

A Proof of Lemma 1

We derive the closed-form expression of the system SCP_s as follows:

$$\begin{aligned} SCP_s &= \Pr\left\{t_{j^*}^{off} < T^{th}, t_{k^*}^{off} < T^{th}\right\} \\ &= \int_B^{\infty} f_y(y)dy \left[1 - F_x(A^{(y)})\right] \\ &\overset{(a)}{=} \sum_{p=1}^{K} \binom{K}{p} \frac{(-1)^{p+1} p}{\lambda_y} \left[\frac{\lambda_y e^{-\frac{p}{\lambda_y}B}}{p}\right. \\ &\left. - \frac{\pi b}{2Z} \sum_{k=0}^{J} \binom{J}{k} (-1)^k \sum_{z=1}^{Z} \sqrt{1-(\zeta_z)^2} e^{-\frac{k}{\lambda_x}A} \omega_z{}^{\frac{p}{\lambda_y}-1}\right] \end{aligned} \tag{8}$$

where $A^{(y)} = \sqrt{\frac{\sigma_A[a_2 y^2 + a_3]}{a_1}}$, $B = \sqrt{\frac{\sigma_B a_5}{a_4}}$, $b = e^{-B}$, $\zeta_z = \cos\left(\frac{\pi(2z-1)}{2Z}\right)$, $A = \sqrt{\frac{\sigma_A[a_2(-\ln(\omega_z))^2 + a_3]}{a_1}}$, $\omega_z = \frac{(\zeta_z+1)b}{2}$, $\sigma_B = 2^{\frac{\mathcal{L}_{k^*}^{off}}{W(T^{th})^2}} - 1$, $\sigma_A = 2^{\frac{\mathcal{L}_{j^*}^{off}}{W(T^{th})^2}} - 1$. Step (a) is achieved by substituting (2), (3), and employing Gaussian-Chebyshev Quadrature [16] with Z as the complexity-vs-accuracy trade-off coefficient.

References

1. J. H. Park, S. C Choi, I. Y Ahn, and J. Kim. Multiple UAVs-based surveillance and reconnaissance system utilizing IoT platform. International Conference on Electronics, Information, and Communication (ICEIC), 2019.
2. F. Vhora and J. Gandhi. A comprehensive survey on mobile edge computing: Challenges, tools, applications. Fourth International Conference on Computing Methodologies and Communication (ICCMC), 2020.
3. Z. Zhang, H. Pang, A. Georgiadis, and C. Cecati. Wireless power transfer – an overview. IEEE Transactions on Industrial., 66:1044 – 1058, 2018.
4. F. Zhou, Z. Li, J. Cheng, Q. Li, and J. Si. Robust an-aided beamforming and power splitting design for secure MISO cognitive radio with SWIPT. IEEE Trans. on Wireless Comm., 16(4):2450 – 2464, 2017.
5. X. Hu, K. K. Wong, and K. Yang. Wireless powered cooperation-assisted mobile edge computing. IEEE Transactions on Wireless Communications, 17(4):2375 – 2388, 2018.
6. A. N. Nguyen, D. B. Ha, V. N. Vo, V. T. Truong, D. T. Do, and C. So-In. Performance analysis and optimization for IoT mobile edge computing networks with RF energy harvesting and UAV relaying. IEEE Access, 23(10):21526 – 21540, 2022.
7. A. N. Nguyen, V. N. Vo, C. So-In, D. Ha, and V. T. Truong. Performance analysis in UAV-enabled relay with NOMA under Nakagami-m fading considering adaptive power splitting. In Proc. JCSSE, Lampang, Thailand, pages 1–6, 2021.
8. P. S. Bithas, V. Nikolaidis, A. G. Kanatas, and G. K. Karagiannidis. UAV-to-ground communications: Channel modeling and UAV selection. IEEE Transactions on Communications, 68(8):5135 – 5144, 2020.
9. F. Zhou, Y. Wu, R. Qingyang Hu, and Y. Qian. Computation rate maximization in UAV-enabled wireless-powered mobile-edge computing systems. IEEE Jour. on Selec., 36(9):1927 – 1941, 2018.
10. L. Dai, B. Wang, Y. Yuan, S. Han, I. Chih-lin, and Z. Wang. Non-orthogonal multiple access for 5G: solutions, challenges, opportunities, and future research trends. IEEE Communications Magazine, 53(9):74 – 81, 2015.
11. V. T. Truong, D. B. Ha, Y. Lee, and A. N. Nguyen. On performance of cooperative transmission in uplink non-orthogonal multiple access wireless sensor networks. International Conference on Recent Advances in Signal Processing, Telecommunications and Computing (SigTelCom), pages 56–60, 2020.
12. N. R. Kota and K. Naidu. Minimizing energy consumption in H-NOMA based UAV-assisted MEC network. IEEE Communications Letters, 27(9):2536 – 2540, 2023.
13. Y. Gao, B. Xia, Y. Liu, Y. Yao, K. Xiao, and G. Lu. Analysis of the dynamic ordered decoding for uplink NOMA systems with imperfect CSI. IEEE Trans. Veh. Technol., 67(7):6647–6651, 2018.
14. F. Kara and H. Kaya. Improved user fairness in decode-forward relaying non-orthogonal multiple access schemes with imperfect SIC and CSI. IEEE Access, 8:97540–97556, 2020.
15. T. Zhang, Y. Xu, J. Loo, D. Yang, and L. Xiao. Joint computation and communication design for UAV-assisted mobile edge computing in IoT. IEEE Transactions on Industrial, 16(8):5505 – 5516, 2020.
16. K. L. Judd. Quadrature methods presented at university of Chicago's initiative for computational economics. 2012.